18th International Conference on Space Operations, Montreal, Canada, 26 - 30 May 2025.

SpaceOps-2025, ID # 388

Innovative Ground Testing of CubeSat ADCS for Advancing CubeSat Reliability

Ali Al-Qaraan[a]*, Ahmed Bushlaibi [b], Ashraf Khater [c], Marwan Almeer [d]

[a] *National Space Science Agency, Kingdom of Bahrain, ali.alqaraan@nssa.gov.bh*
[b] *National Space Science Agency, Kingdom of Bahrain, a.bushlaibi@nssa.gov.bh*
[c] *National Space Science Agency, Kingdom of Bahrain, ashraf.khater@nssa.gov.bh*
[d] *National Space Science Agency, Kingdom of Bahrain,* marwan.almeer@nssa.gov.bh
* Corresponding Author

Abstract

CubeSats have transformed space exploration by offering lower manufacturing and operational costs, making them accessible to research and academic institutions. Ensuring their functionality and reliability before launch is critical, as on-orbit maintenance is not feasible. Ground testing of the Attitude Determination and Control Subsystem (ADCS), a complex and essential component of satellites, is particularly challenging. Traditional ADCS testbeds are often expensive, complicated to operate, and fail to replicate the frictionless space environment. Magnetic levitation systems, while promising for ADCS testing, are inherently non-linear, complex, and expensive, posing significant design challenges. This work aims to reduce the cost and complexity of magnetic levitation systems by developing a financially feasible testbed enclosed in a Helmholtz cage, designed to generate a uniform magnetic field to simulate earth's magnetic field. The magnetic levitation system includes a feedback control mechanism based on a Proportional-Derivative (PD) controller and a single linear Hall-effect sensor for distance measurement. The system was modeled and simulated to design and tune the controller, achieving stable levitation in simulations. However, experimental results highlighted the limitations of the Hall-effect sensor due to noise and susceptibility to external magnetic fields, leading to unstable responses. These findings suggest that multiple Hall-effect sensors or optical displacement sensors could enhance measurement accuracy and system stability. This study demonstrates the potential of simplified magnetic levitation systems for CubeSat ADCS testing and provides a pathway for addressing the inherent challenges of such designs.

Keywords: CubeSat, ADCS, Magnetic Levitation System, Helmholtz Cage, PD Controller, B-dot Algorithm, Space Environment Simulation

Nomenclature

This section is not numbered. A nomenclature section could be provided when there are mathematical symbols in your paper. Superscripts and subscripts must be listed separately. Nomenclature definitions should not appear again in the text.

Acronyms/Abbreviations

ADCS	Attitude Determination and Control Subsystem
MLS	Magnetic Levitation System
PD	Proportional-Derivative
HIL	Hardware-in-the-Loop
CubeSat	Cube Satellite
ORF	Orbit Reference Frame
BOF	Body Reference Frame
P-POD	Transceiver
MTQ	Magnetorquer
IGRF	International Geomagnetic Reference Field
ECEF	Earth-Centered Earth Fixed Frame
GCI	Geocentric Inertial Frame
PWM	Pulse Width Modulation

1. Introduction

As electronic components become more compact and affordable, numerous technological systems are able to produce equal or improved results with smaller form factors and reduced costs. This rapid technological evolution has enabled educational and commercial entities to enter fields once dominated by government research institutions. One such field is space technology, where the miniaturization of satellites has shifted industry focus toward low-cost, quickly deployable, high-performance missions. CubeSats, a class of nanosatellites, embody this shift and have gained popularity due to their ease of adaptation, reduced development times, and cost-effective launch operations. The CubeSat standardized bus structure is among the most used configurations for nano- and pico-satellite missions **Error! Reference source not found.**. This standardized framework allows developers to concentrate on payload design, streamlining the preparation and launch processes. Consequently, a marketplace for off-the-shelf CubeSat subsystems has emerged, with components ready to be integrated into the CubeSat bus. Within these subsystems, the Attitude Determination and Control Subsystem (ADCS) is particularly critical. The ADCS subsystem is responsible for orienting the satellite's instruments, such as optical detectors and communication antennas, toward specified targets to meet mission requirements. Given the high costs associated with CubeSat launches, extensive pre-launch testing is essential. Unlike larger satellites, CubeSats typically lack onboard maintenance capabilities, meaning any in-orbit failures cannot be easily rectified. This drives the need for rigorous ground testing of all subsystems, especially the ADCS, which plays a crucial role in satellite stability and orientation during missions.

1.1 Subsection headings

Subsection headings are in *italics* and placed flush on the left-hand margin of the column.

1.1.1 Sub-subsection headings

Sub-subsection headings are in *italics* and placed flush on the left-hand margin of the column.

1.1. Problem Statement

The objective of this work is to design, build, and test an ADCS framework for CubeSats with a 1U standard size (10 cm x 10 cm x 10 cm) and a maximum weight of 2.6 kg. This testing framework will simulate in-orbit conditions to evaluate the ADCS subsystem's performance using simulations and Hardware-in-the-Loop (HIL) environments. Such a framework is essential to ensure CubeSat reliability and mission success

1.2. Research Objectives

This study's main goal is to create a CubeSat testing platform to validate ADCS algorithms and hardware within an HIL environment. This platform aims to provide a realistic testing environment that combines magnetic levitation and uniform magnetic fields for evaluating CubeSat ADCS performance. Specific objectives include:

1. Designing and constructing a Helmholtz cage that can simulate the Earth's magnetic field along one axis.
2. Building a Magnetic Levitation System (MLV) to provide a frictionless environment that enables free rotation around an axis orthogonal to the magnetic field vector produced by the Helmholtz cage.
3. Testing attitude estimation and control algorithms, with a focus on the B-dot control algorithm to assess its effectiveness in managing CubeSat orientation and stability

2. Literature Review

The CubeSat standard, developed through collaboration between California Polytechnic State University (Cal Poly) and Stanford University, aims to provide a framework for creating standardized picosatellites with low-cost, quick turnaround builds. However, ground testing of CubeSat ADCS remains challenging due to the difficulty of replicating frictionless, on-orbit conditions on Earth. Academic research has explored a range of ADCS testbeds, but these systems are often hindered by high costs, complexity, and limited frictionless simulation capabilities. While air-bearing platforms offer low-friction environments, they present challenges related to precise center-of-mass alignment and are susceptible to air current disturbances. A promising alternative is electromagnetic levitation, which provides near-frictionless motion for 1-degree-of-freedom ADCS testing. Mire-Hicks F, Lozano from Massachusetts Institute of Technology (MIT) applied magnetic levitation in testing electrospray thrusters (iEPS) for cube satellites [1]. In their work, a vacuum chamber has been used to test the iEPS thrusters which can operate only in vacuum environment [1]. Their setup can be seen in **Error! Reference source not found.**. Their setup is attributed with complexity and expensiveness.

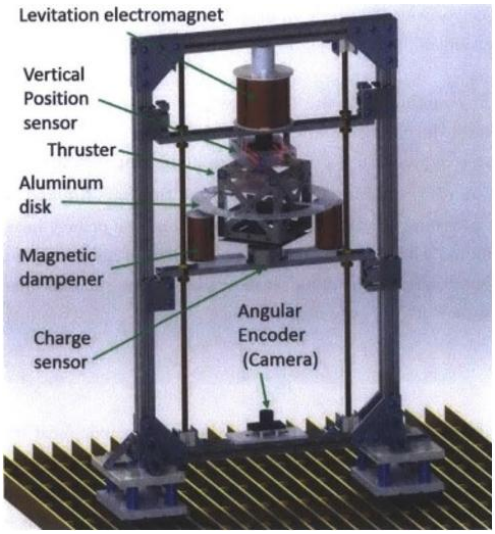

Figure 1 MIT MLS Setup

Although such testbeds are effective, few research efforts have applied magnetic levitation to CubeSat magnetic control systems, representing a gap this study aims to address by combining a magnetic levitation system with a Helmholtz cage for CubeSat testing. Also, trying to provide simpler design than the one used in MIT for testing electrical power system would ensure that the testbed is within the reach of most academic institutes.

3. **Theory and Calculation**

A Theory section should extend, not repeat, the background to the article already dealt with in the Introduction and lay the foundation for further work. In contrast, a Calculation section represents a practical development from a theoretical basis.

3.1 Magnetic Levitation

Magnetic Levitation systems (MLS) are used in many applications and systems in the modern world such as Maglev trains and magnetic bearings [2,3]. Also, it is a subject that is characterized with high research and development potential that has attracted many researchers [3]. Many mechanical systems have inherited problems that reduce their efficiency, causes wear, tear and increase maintenance costs of the system such as friction and mechanical movements and vibration [3]. MLS on the other hand, gained reputation due the contactless and frictionless features they provide which reduced or eliminated the mentioned earlier mechanical problems [3]. MLS objective – in simple words- is to suspend and retain a mass in free space by magnetic force and without the aid of any physical support ensuring certain degree of freedom [3].

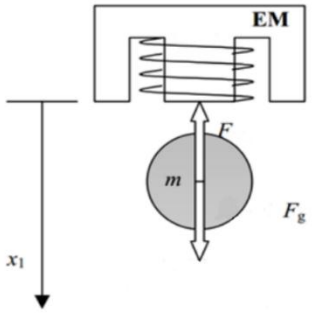

Figure 2 Magnetic Levitation system force diagram

According to Earnshaw theorem, using only permanent magnets, it is impossible to establish a stable, stationary levitation [4]. To overcome this limitation, MLS requires the usage of actively controlled electromagnet as an actuator with a suitable sensor through a feedback loop as in **Error! Reference source not found.** [4]. MLS can be classified into two types according to the type of magnetic force it can produce: namely, repulsive and attractive forces [3]. The type of forces required are selected depending on the application, orientation of the setup and the object to be suspended.

MLS are considered intrinsically unstable in an open-loop control system [3]. Moreover, by nature, these types of systems behave in a highly non-linear fashion as shall be discussed in the implementation section [4]. These two features will result in complex, highly non-linear dynamical equations for the system which will require an accurate model of the system and designing a highly efficient, accurate and robust feedback control system to achieve stable levitation of the object [3]. Designing the system will be discussed in detail in the coming sections.

3.2 System Design and Implementation

For this study, the testing setup comprises a Helmholtz cage and a Magnetic Levitation System (MLS). The Helmholtz cage is designed to simulate the Earth's magnetic field by generating a uniform magnetic field of ±2% within a 12 cm region, using coils with 98 turns each to produce the desired magnetic field strength under controlled current conditions. A single-axis cage configuration is used for simplicity and cost-efficiency, and this configuration suffices for testing CubeSat ADCS in a realistic magnetic environment.

To maintain a frictionless environment, an air gap of 0.3 mm shall be established using a Proportional-Derivative (PD) control system with a Hall-effect sensor for distance measurement. The MLS setup was first simulated in Simulink to verify the system's feasibility, and empirical tests were then conducted to establish a correlation between the applied current and the electromagnetic force produced. To achieve system stability, PD control parameters were tuned through a series of trial-and-error adjustments. This MLS configuration provides a low-friction test environment that closely approximates space conditions, allowing accurate testing of ADCS algorithms like the B-dot algorithm

4. Designing Magnetic Levitation Control System

In this section the design and implementation of the magnetic levitation is presented. First, a detailed explanation of MLS control system including mathematical derivation of the blocks of the control system. Then, Electrical schematics design, component selection and controller design and implementation will be presented.

4.1 Block Diagram Model

MLS control system block diagram can be seen in **Error! Reference source not found.**. It can be seen from the figure that the controlled variable is the distance ($\boldsymbol{x}$) between the electromagnet and the levitated object, which is basically the objective of MLS in general. The distance is measured using Hall-effect sensor which will measure the magnetic field strength from the permanent magnet which depends on the distance between the two as discussed earlier. The measured signal will be processed using a filter which will provide noise free signal to the comparator. Since this is a regulating control problem, the comparator will subtract the measured distance from the set point, or the required distance to be maintained, or provided by the user, to produce an error term. The error term is fed to a micro controller where various control algorithm can be applied to produce the required control signal to the actuator. Current (I) is the variable directly proportional to controlling the distance (x) through the force produced by the electromagnet(f_{mag}). However, to control the current, Pulse Width Modulation (PWM) signal is required to control the current in the

winding. The PWM signal will be fed to into a switching circuit which interfaces the PWM signal from the microcontroller and the DC power supply.

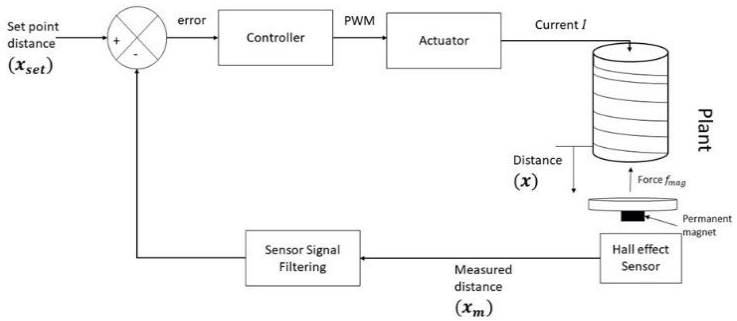

Figure 3 MLS Block Diagram Model

Modeling the system

When modelling MLS systems, the focus is on modelling Electromagnetic coils which are usually looked as an RL circuit as inductors show resistive behaviour especially with high frequency switching **Error! Reference source not found.**

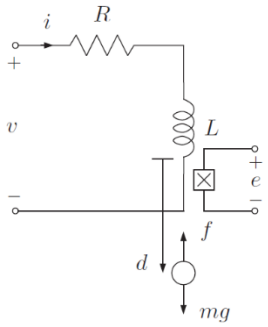

Figure 4 MLS RL Model

Based on Kirchhoff's law, the first differential equation of the system

$$v(t) = v_R + v_L$$

where $v(t)$, v_R and v_L are the input voltage and the voltages across the resistive and inductance part of the coil. Eq. (38) can be rewritten as

$$v(t) = Ri + \mathrm{L}\,\frac{di}{dt}$$

Transforming this equation into transfer function in s-domain with the voltage $v(s)$ as the input and the current $i(s)$ as the output:

$$G = \frac{i(s)}{v(s)} = \frac{1}{Ls+R}$$

Looking into the mechanical model of the system, for levitating an object, the electromagnet must produce a force which is equal to gravitational force however oppose it. Using Newton's second law:

$$F_{total} = F_{grav} + f_{mag}$$

$$m\ddot{x} = mg - f_{mag}(x, i)$$

which can be rewritten in the differential equation from:

$$\ddot{x} = g - \frac{f_{mag}(x,i)}{m} \quad (6)$$

The electromagnetic force $f_{mag}(x,i)$ is a variable of distance and current and is not easy to be determined due to the complexity and nonlinearity relation between the variables. Also, the usage of ferrite pot core will introduce difficulty in calculating the associated parameters related to the core geometry. Thus, to establish the relation between electromagnetic core, distance and current, experimental testing was conducted to find the empirical equation that relate these parameters as will be discussed later.

4.2 Open-loop Model

The electrical open-loop model which shows the relation between electromagnet current output and the PWM voltage input can be seen below in **Error! Reference source not found.** along with the simulation parameters used in **Error! Reference source not found.**:

Table 1 Simulation Parameters

Inductance (H)	0.3246H
Resistance (Ω)	19.5Ω
PWM frequency	10kHz
Duty Cycle	50%

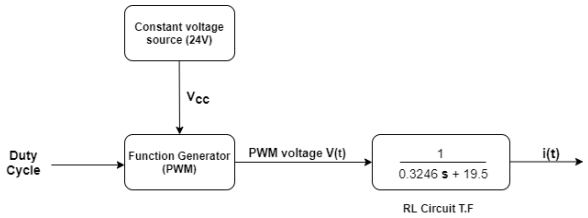

Figure 5 Electrical Model of the system

The parameters were selected to be similar to the specifications of the implemented system. The inductance and resistance are those of the electromagnetic core used in the implementation phase. The transfer function G(s) was used to represent the electromagnet model and convert the input PWM voltage into the current output as can be seen in Figure 6

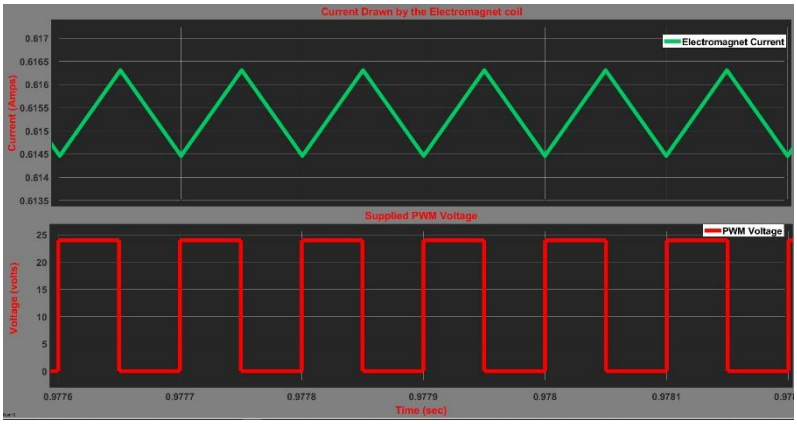

Figure 6 Current Drawn by Electromagnet Coil (Amperes vs Time) and the Supplied PWM voltage (Volts vs Time)

The output current has transient response as can be seen from **Error! Reference source not found.** Although the value of the current varies between 0.6144A and 0.6164A, however, the effective current is the average current from the steady-state value 0.6154 Amps (50% Duty Cycle) as in **Error! Reference source not found.**. The maximum current reached was 1.127A when the duty cycle is 100% or 24V throughout the simulation period.

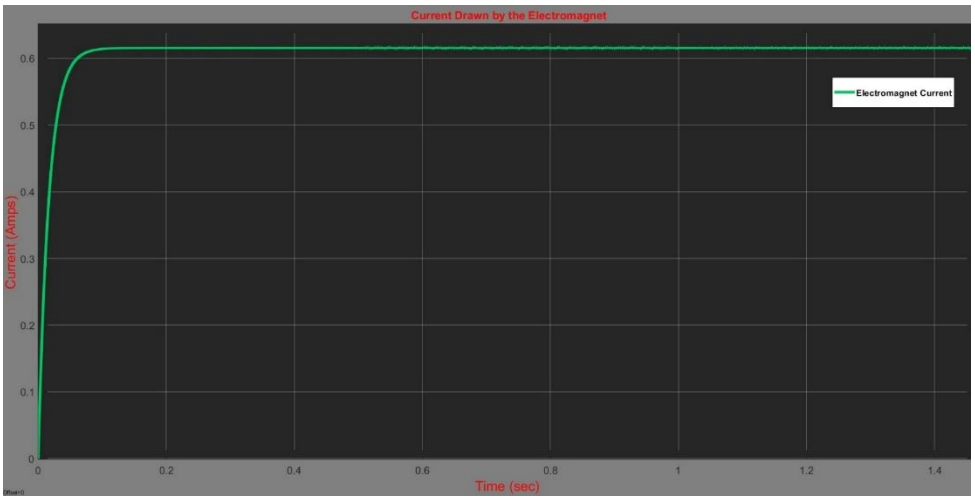

Figure 7 Current Drawn by the Electromagnet for 100% Duty Cycle (Current (Amps) vs Time (sec))

4.3 Closed-Loop System Model

To have a comprehensive overview of the system, a simplified close-loop model with P controller only was built. a resulted empirical equation from the electromagnet force experiment was utilized as a block in the model which takes the value of (K= N*I) as an input and convert it to a force. The resulting force is scaled by the square of the distance to compensate for the fact that the relation between the magnetic force and the distance follows the inverted square law [5].

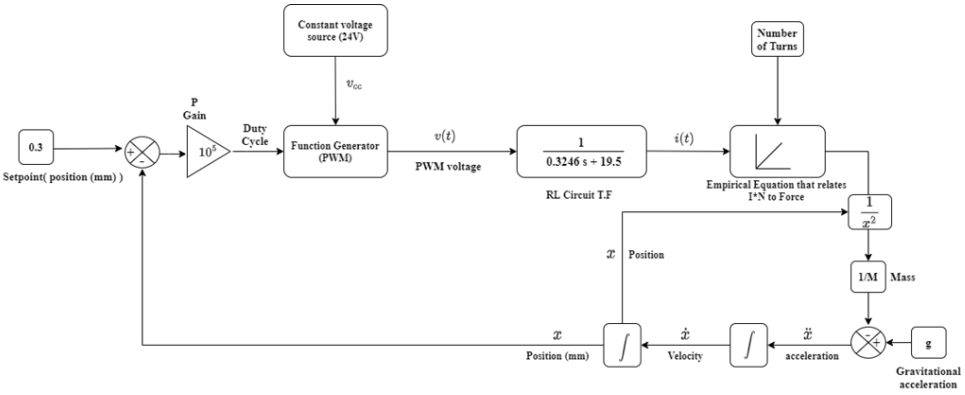

Figure 8 Close-loop System Model with P controller only

The system is inherently unstable and highly nonlinear due to many variables such as the nonlinear relation between the force produced by the electromagnet and the length of the air gap and the nonlinear relation between the inductance

of the electromagnet and the length of the air gap between the ferromagnetic cores. Thus, with a simple closed loop system using only proportional gain, a stable response, would be unattainable. Figure 9 represents the distance between the upper electromagnet and the lower ferrite core while using only proportional (P) controller.

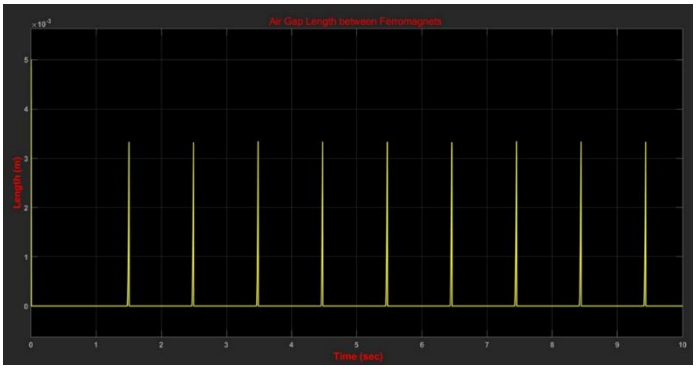

Figure 9 Air Gap Length between Ferromagnetic cores using P controller (Length (m) vs Time (sec))

It is noticeable from Figure 9 that the distance is not stable and the setpoint (3mm) was only momentarily achieved with some error. To achieve a stable response, proportional-derivate (PD) controller was used. The design and tuning process are discussed in the controller design section.

4.3.1 Empirical Equations

Two relations in this work were obtained using experimental testing. The first equation is the relation between the electromagnetic force $f(x,i)$ and current for certain distance. The second equation is the relation between the magnetic field measurement from the Hall-effect sensor and the distance between the sensor and the permanent magnetic which reflects the distance between the electromagnet and the ferromagnetic core it tries to levitate.

4.3.1.1 Electromagnetic Force

To determine the electromagnetic force, an experiment is conducted by inserting a 1mm thick plastic plate between the electromagnet and the ferromagnetic core. This test provides an insight of the relation between force and distance, however; it differs due to the fact that in the final implementation, the gap will be an airgap which has different magnetic permeability from plastic. The test was conducted by adding different weights and measuring the current required to hold these weights.

Table 2 shows the testing parameters. The selection of 1 mm gap between the electromagnetic core and ferrite core was for sake of testing the worst-case performance of the system where the gap is more than double the required 0.3mm setpoint, thus, losing more than squared the magnetic force produced.

Table 2 Force (trial 1) Test Parameters

Magnetic Wire Diameter (mm)	Gap between cores (mm)	No. of Turns	Resistance (Ω)
0.511	1mm	191	2.47

And the following data was collected from the experiment:

Table 3 Force (trial 1) results

Current (A)	Max weight (g)	K = I*N	Power loss = I^2*R (W)	Current Density A/mm^2
0.69	170	131.79	1.175967	3.364475802

2.15	1530	410.65	11.417575	10.48351156
2.57	1870	490.87	16.314103	12.53145335
2.9	2000	553.9	20.7727	14.14055047

The same test was conducted with smaller magnetic wire. The testing parameters are shown in Table 7:

Table 4 Force (trial 2) test parameters

Magnetic Wire Diameter (mm)	Gap between cores (mm)	No. of Turns	Resistance (Ω)
0.32	1mm and 0mm	430	12.45

The following data shown in Table 8 was collected from the second experiment:

Table 5 Force (trial 2) results

	Current (A)	Max weight (g)	K = I*N	Power loss = I^2*R (W)	Current Density A/mm^2
	0.33	170	141.9	1.355805	4.103213377
	1.1	1530	473	15.0645	13.67737792
0mm gap	0.16	5000	68.8	0.31872	1.989436789

It can be noticed from the results tables that 0.511mm thick wire required less current to carry the same weight than the 0.32mm thick wire although it has more turns. Also, the 0.511mm wire has less power loss compared to the other wire and it has lower current density which is very important in the heating issue. For these reasons, the selection of wire with a diameter higher than 0.33mm is required or we can use the similar wire with increasing the number of turns.
For finding the electromagnetic force, the collected data for K against the gravitational force were plotted and fitted to a curve using Matlab® curve fitting toolbox. The fitting results can be seen in Figure 9

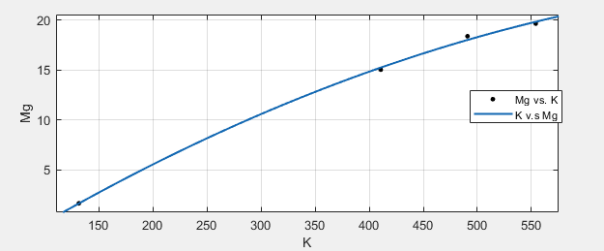

Figure 10 K vs Mg Curve Fitting

The reason behind selecting K in this relation instead of the current directly is to attenuate the effect of number of turns from the supplied current in case another coil with different number of turns is used. Moreover, the value of (K= I*N) is directly proportional to both magnetic field B and electromagnetic force produced $f_{mag}(x,i)$ according to Biot Savart Law. The plotted data was fitted to a second-degree polynomial. The equation the goodness of fitting statistics can be seen below

Table 6 Goodness of Fit Statistics

The sum of squares due to error (SSE)	0.2076
R-square	0.999
Adjusted R-square	0.9969
Root mean square error	0.4557

The model of the equation is

$$f_{mag}(i) = \alpha x^2 + \beta x + \gamma$$

Where, the coefficients α, β, γ are as shown in Table 7

Table 7 Model equation coefficients

Coefficient	Value
α	-3.951×10^{-5}
β	0.07006
γ	-6.895

The resulted equation shall be used in simulating the whole system and the close-loop control system in later section

4.3.1.2 Relation between Magnetic Field Strength and Distance

Hall-effect sensors are usually used to measure the strength of magnetic field. However, in this work it will be used to measure the distance between the sensor itself and the permanent magnet which will be installed under the levitating object. According to the datasheet of the sensor, there is a linear relation between the measured magnetic field and the output voltage of the sensor as shown in Figure *11*

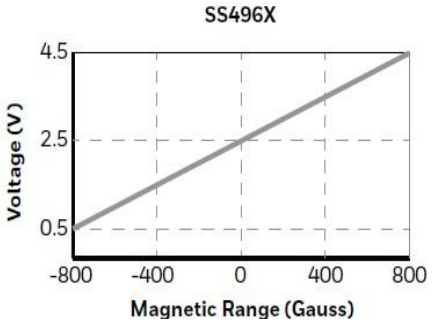

Figure 11 Hall-Effect Sensor Linear Relation between Mag. Field and the Output voltage [6]

Although this relation is linear, the relation between the magnetic field strength with distance is not linear and it follows the inverse square law, which means if we increase the distance twice, the resultant magnetic field strength reduced by quarter as shown in Figure 12 [5]. Thus, it is important to operate the MLS system around the linearized region of the relation between the magnetic flux density and the distance.

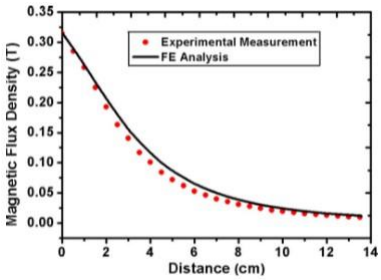

Figure 12 The relation between magnetic flux and Distance [5]

To find the relation, an experimental setup was made to hold both the sensor and the magnet at each end of the setup. Micro-inch movements were induced and the reading from sensors were logged. The Hall-effect sensor was connected to Arduino Mega 2560 which reads the Hall-effect voltage outputs and convert them to digital reading through 10-bit analog to digital converter (ADC), which means that the operating voltages will be mapped into an integer between 0 and 1023 with a sensitivity of 4.9mV for 5V input. For every distance, fifteen measurements were taken to check the consistency of the readings as can be seen from a sample of the data collected in Table 8.

Table 8 Experimental Results from Hall-effect Sensor

Readings	Distance between sensor and magnet (mm)				
	0.40	0.46	0.52	0.58	0.76
	105	114	126	128	138
	105	116	129	128	137
	107	115	126	127	137
	104	115	125	130	138
	104	115	128	131	138
	105	113	126	130	138
	106	115	129	132	136
	108	115	128	128	141
	104	114	128	127	137
	105	114	127	130	138
	107	114	127	128	139
	105	113	128	128	137
	105	116	127	128	137
	106	113	128	129	137
	105	114	127	128	136

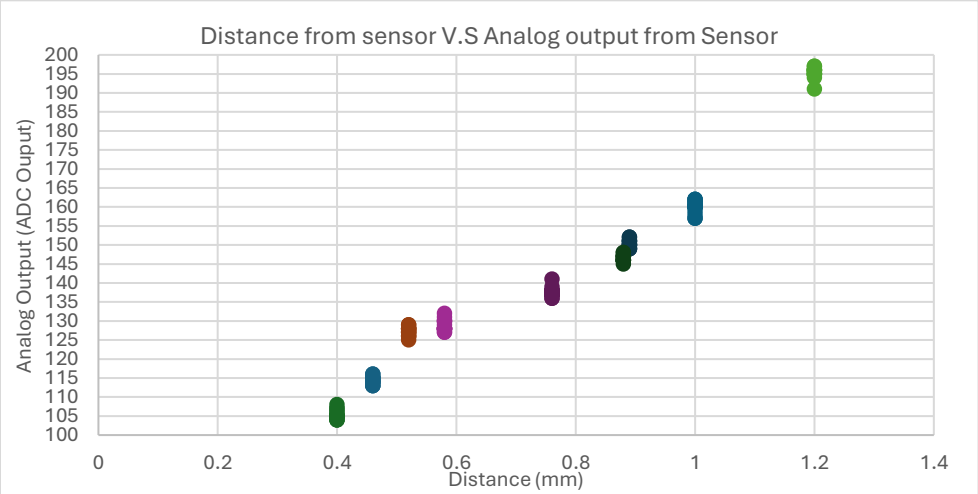

Figure 13 Plot of the Hall Effect Sensor Data output for variable distances

It can be seen from Figure *13* that for every distance there is variation in the reading of the sensor within certain ranges. Some of the ranges has some overlapping which can cause issues for the microcontroller to interpret the distance from these readings. Thus, to solve this issue, moving average filter was implemented. Moving average filters are the easiest and optimal filters that can be used for time domain processes. The equation of the filter is as follow

$$y(i) = \frac{1}{P}\sum_{j=0}^{P-1} x[\,i + j]$$

Where the P is the number of points to be averaged, x and y are the input distance and the output voltage from the sensor, respectively. In this work, averaging was experimented with 5 and 15 points to understand the optimal fitting. The values were also rounded to the nearest integer as can be seen the graph below.

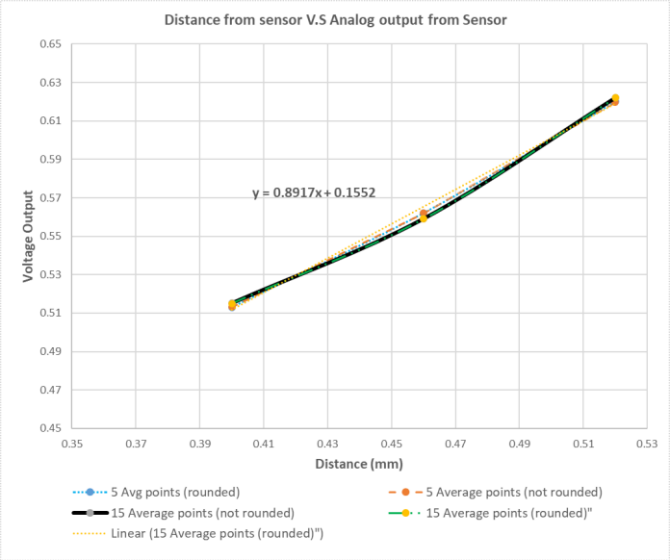

Figure 14 Plot of the Hall Effect Sensor Data Using Different Number of Moving Average Points

It can be seen from the plot that 5 points and 15 points moving averages do not deviate significantly from each other, thus 5 points moving average is considered in this work. The points were fitted with a linear relation and produced the following equation

$$y = 0.8917x + 0.1552$$

Although this linear relation and change in voltage with respect to the change of distance may suffice for some applications, the range is not useful in our case. Thus, stronger magnets were used to provide bigger change in voltage associated with small change in distance. Moreover, stronger magnets can eliminate the problem of fluctuation in readings and can provide wider range. Using stronger magnets will help in fitting the linear relation of the sensor into a linear region of the relation of magnetic field with distance. To find the equation using stronger magnet, micrometre screw with 0.04mm resolution was used to measure accurately the output of the Hall-Effect sensor at 0.5 distances. The results obtained are shown in **Error! Reference source not found.** and Figure *15*.

Table 9 Distance vs Voltage

Distance (mm)	Voltage(volts)
10	4.480
10.5	4.336
11	4.210
11.5	4.097
12	3.992
12.5	3.891
13	3.804
13.5	3.725
14	3.650
14.5	3.580

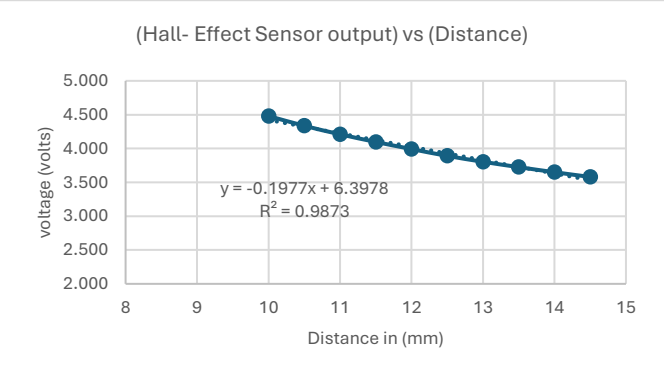

Figure 15 Relation between (Hall-effect readings vs distance) using stronger magnet

The sensor is operating in the upper region – between 2.5 and 4.5 Volts- compared to the previous test. It is important to clarify that data in **Error! Reference source not found.** is the average between 3 points as the readings suffered from fluctuations. The equation of the plotted line was used in the final code.

4.3.1.3 Electrical Schematic

The electrical schematic of the system which was implemented can be seen in Figure *16*. It can be noticed from the schematic that a Schottky diode was added parallel to the electromagnetic coil. The reason is to prevent fly back voltage spikes which have significantly higher voltage than the power source. To increase the accuracy of the voltage reading from the Hall-effect sensor, external 16-Bit ADC module was used to interface the sensor to the microcontroller. This module can provide 0.152mV resolution for 5V input.

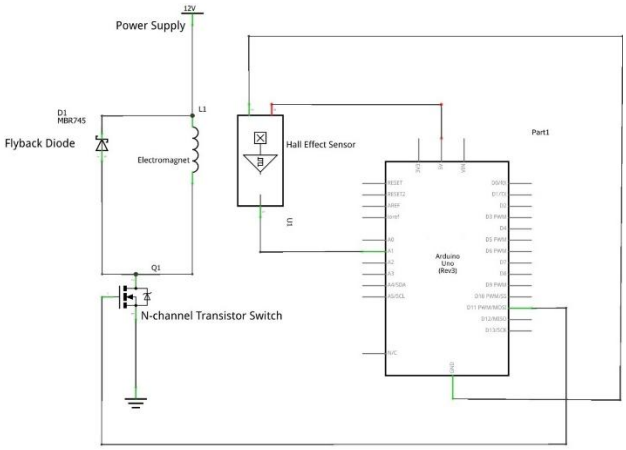

Figure 16 Electrical Circuit Schematic

4.3.1.4 Selected Components

For implementing the MLS system, the following components were selected:

- Coil Core

Electromagnets ferrite cores can take many geometries and sizes. They are used to strengthen and concentrate the magnetic field produced by the coil. For this work, the selected core is a pot core which is good in protecting the magnetic field from electromagnetic interference EMI and its geometry is suitable for magnetism. As the actuating signal is a 10 kHz PWM signal, it was critical to consider a core able to withstand higher than this frequency. The specifications of the pot core can be seen in the **Error! Reference source not found.** below

Table 10 TDK N22 Pot Core Specifications

Pot core (half) By TDK®	
Material	N22
Base Material	MnZn
Frequency Range	20-200 kHz
Initial Relative Permeability	2300

1. It can be seen form **Error! Reference source not found.** that the core is able to withstand 20 times the operating PWM signal. The dimensions of one half of the core are as in **Error! Reference source not found.**.

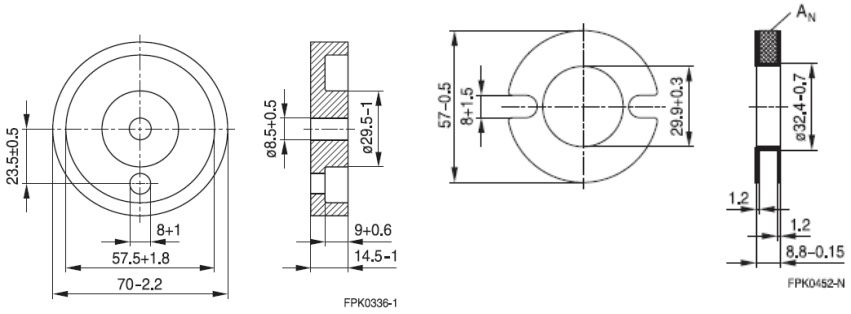

Figure 17 Pot Core and its Bobbin Dimensions

- Magnetic Wire

For the coil magnetic wire, different coils with different magnetic wire sizes were winded manually. The selection of the coil used was determined by the magnetic force test mentioned earlier and verified by the results of model simulations. The following Table 11 has the magnetic wire sizes used in winding.

Table 11 Magnetic Wires Used in the Coils

Wire Diameter (mm)	Max Current (Ampere)	No. of Turns
0.175	≈0.3	1800
0.25	0.86	875
0.315	1.4	570
0.45	2.2	298

- Switching Element

The PWM signal from the microcontroller was interfaced with the power supply through MOS transistor switch. The requirement for this device is to be capable of handling high voltage and relatively high currents and high PWM frequencies. The selected components have the following parameters presented in **Error! Reference source not found.**.

Table 12 MOSFET Transistor Specifications

Type of Transistor	MOSFET
Type of Control Channel	N-Channel
Maximum D-S voltage	40 V
Maximum Drain Current	50 A

- Micro Controller

It is critical in MLS systems to utilize high frequency PWM signal. This will ensure smooth current transition is supplied to the coil, thus allowing precise control over the system. Also, higher switching frequency means less power loss and less mechanical vibration. The requirement for the microcontroller is to supply 10 kHz PWM signal. Thus, for this work, Arduino Mega 2560 will be used as the main microcontroller. Arduino Mega which is built on the ATmega 2560 controller commonly provide 490 Hz which is too small compared to the required frequency. Thus, to

provide the required frequency, timer 1 of the microcontroller was reprogrammed by manipulating the last four register bits of the timer which are associated with a prescaler or division factor that allows the production of the required PWM signal as can be seen inFigure *18*. Timers are usually associated with the system clock which has 16MHz frequency. Timer 0 was not selected for this task as it is assigned by default with main timing functions of controller such as delay() or millis().[7]
After manipulating the timer, the microcontroller produced a 10kHz PWM square signal as in **Error! Reference source not found.**.

Bit	7	6	5	4	3	2	1	0	
(0x61)	CLKPCE	–	–	–	CLKPS3	CLKPS2	CLKPS1	CLKPS0	CLKPR
Read/Write	R/W	R	R	R	R/W	R/W	R/W	R/W	
Initial Value	0	0	0	0	See Bit Description				

Figure 18 Clock Pre-scale Register

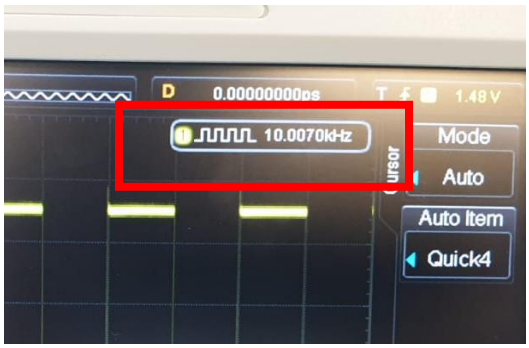

Figure 19 The Produced 10kHz PWM signal from Arduino

4.4 Controller Design and Results
For controlling the response of MLS, PD was used. This has been done instead of the full PID configuration as the introduction of the integral component adds complexities to the system especially with the inherited integral windup problem presented in physical systems. Moreover, eliminating steady-state error is not within the scope of this work.The most challenging part of PID controller implementation is tuning the parameters or the controller gains (K_P , K_D, K_I). Special care must be taken in proposing tuning process as improper tuning process may result in never reaching the stable state of the controller. For this work the following tuning methodology was followed as in Figure *20*

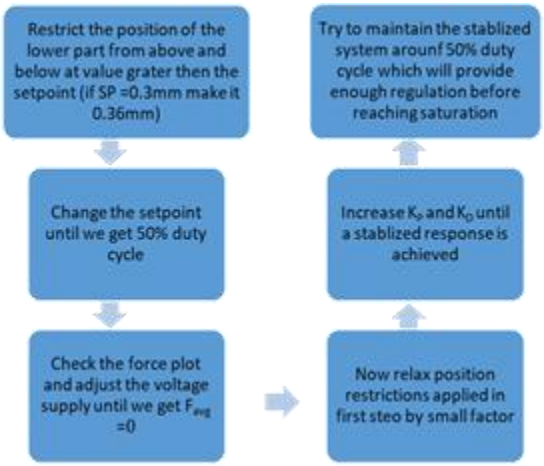

Figure 20 Tuning PD Gains Methodology

Special care must be given to the selected gains of the controller, since in this system the supplied voltage also aids in the overall loop gain. If the voltage was not properly selected, the effect of the gains will be restricted, and the gains will require to be high to stabilize the system. For example, if the controller output was high and the supplied voltage

is low this will lead to the saturation of the controller output in relatively little time interval. For this reason, it was incorporated in the tuning process. After long trial and error tuning process, the following responses were obtained as shown in Figure 21 and Figure 22.

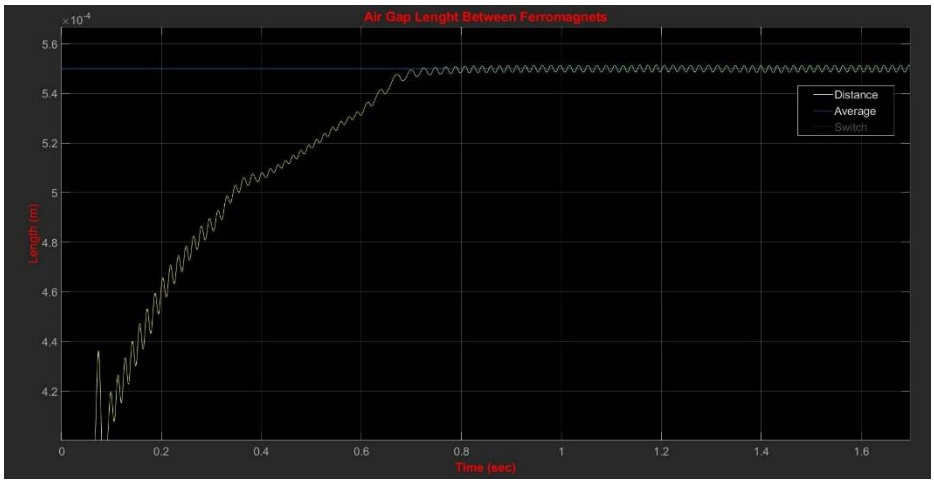

Figure 22 Air Gap Length between Ferromagnetic cores (Length (m) vs Time (s))

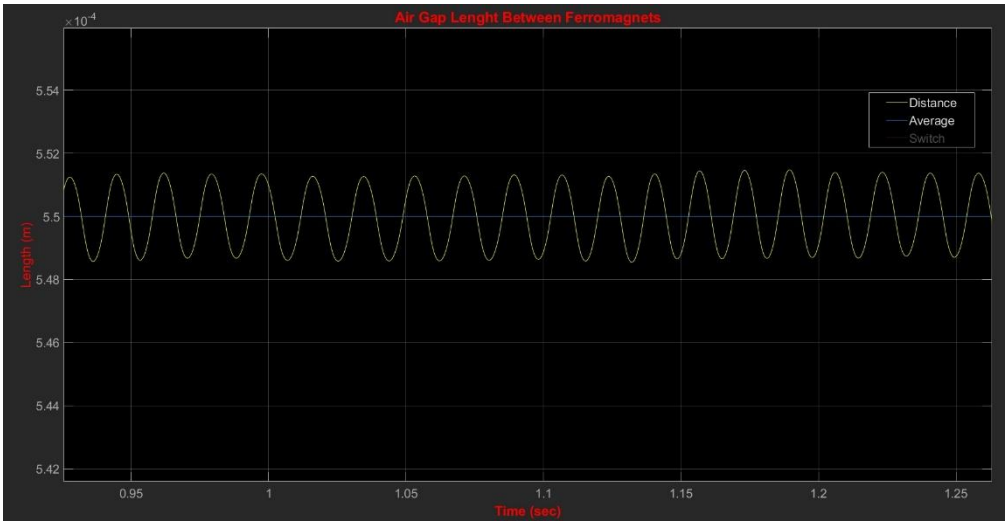

Figure 21 Zoom-in on Steady State Air Gap Length between Ferromagnetic cores (Length (m) vs Time (s))

It can be seen from the position response plots that the levitating base achieved a stable levitation with its position residing in an envelope between 0.549 mm and 0.551mm with an average of 0.550 mm. although the setpoint was 0.3mm, the change in the steady state position is due to not incorporating the integral term of the controller. The fluctuation in the position is due to the PWM signal. The difference between the upper and lower values of the air gap length is 0.002mm which is acceptable in this work. It noticeable that the levitating table was held at 0.4mm initially, this is to prevent saturating the PD gains initially and aids in reducing the required supplied voltage value as the bigger

the air gap is, the more force and thus voltage is required to pull it up. The following Figure *23* represents the response of the PD controller:

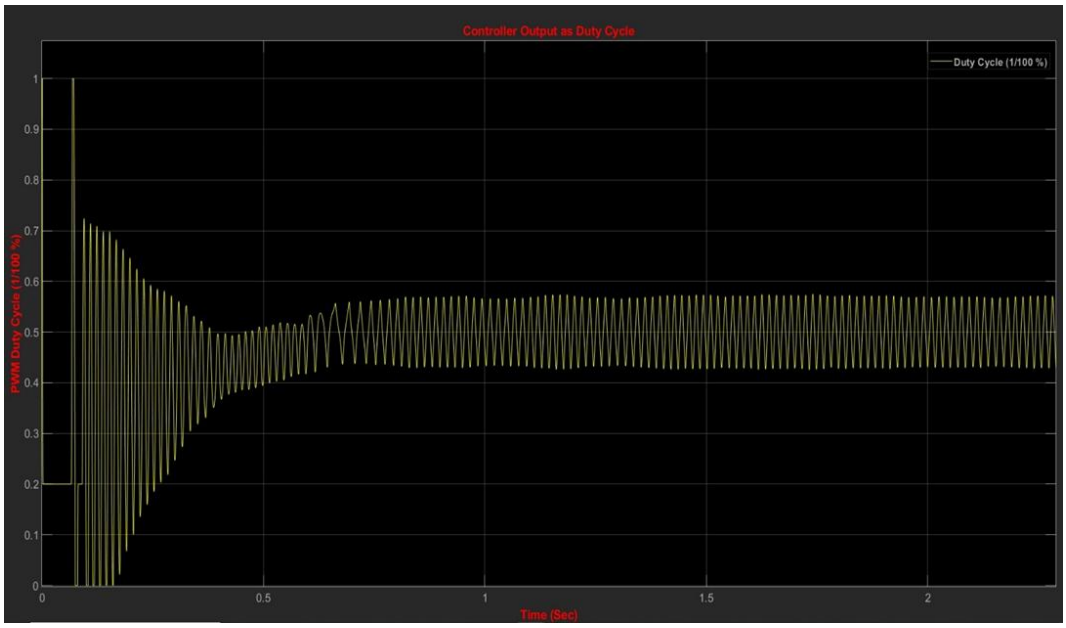

Figure 23 The output of the PD controller is PWM Duty cycle

The output of the PD controller is PWM Duty cycle between [0 and 1] where, 1 is 100% duty cycle. The controller output starts aggressively in the first 0.6 sec as the levitating table starts to fall and the air gap between the ferromagnetic cores increases. During this period, in the real implementation, the levitating base must be assisted by either holding it or adding motion restrictors below it until it passes the transient phase in motion and reaching the steady state region.

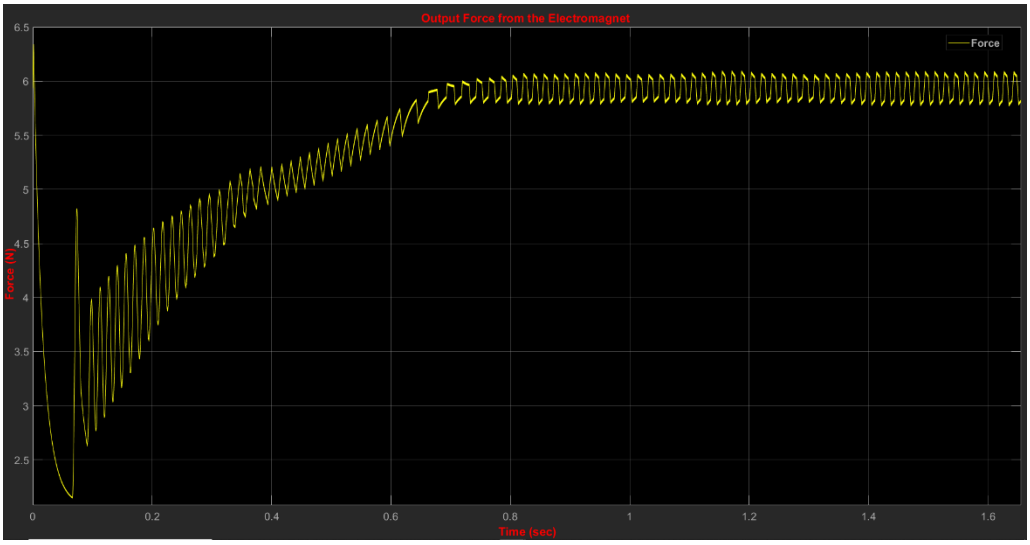

Figure 24 Output Force From the Electromagnet

Similar response is noticeable in the output force from the relation between force and time plot in Figure 24. The force aggressively rises in the first 0.6 sec and reaches the steady state when the levitating base is stably floating with an average value of 5.9 Newton.

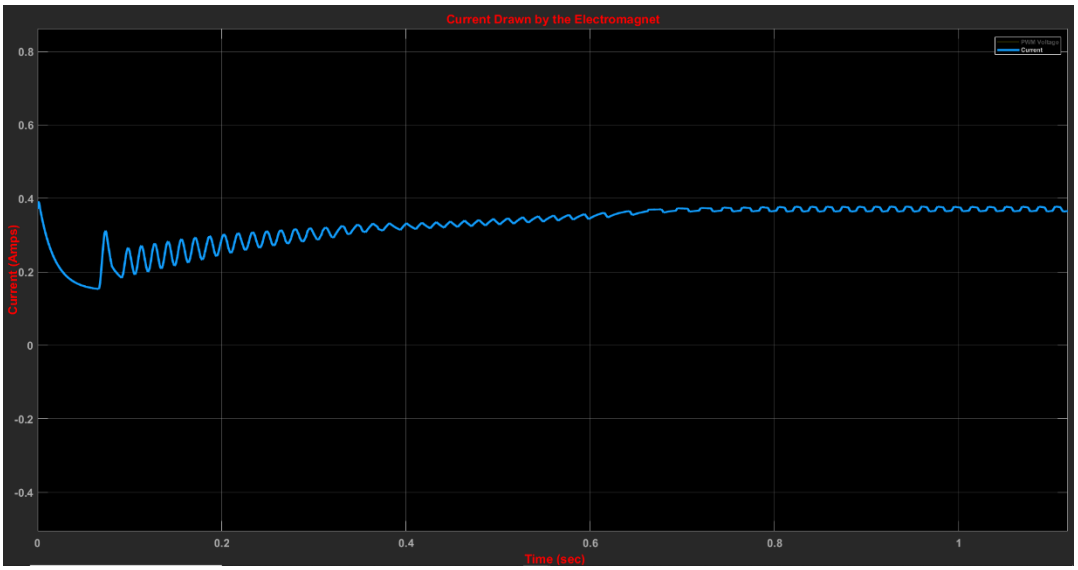

Figure 25 Current Drawn By Electromagnet

The force produced is a function of the current supplied. An initial current of 0.4 A was supplied to the electromagnet to avoid the transient increase in the current which can lead to the levitating base to fall as was shown in the open loop response of the system section at Figure 25. The output of the switching circuit which is the PWM signal generated by the microcontroller scaled by the voltage supplied from the power supply- here 14.4 V- can be seen **Error! Reference source not found.**.

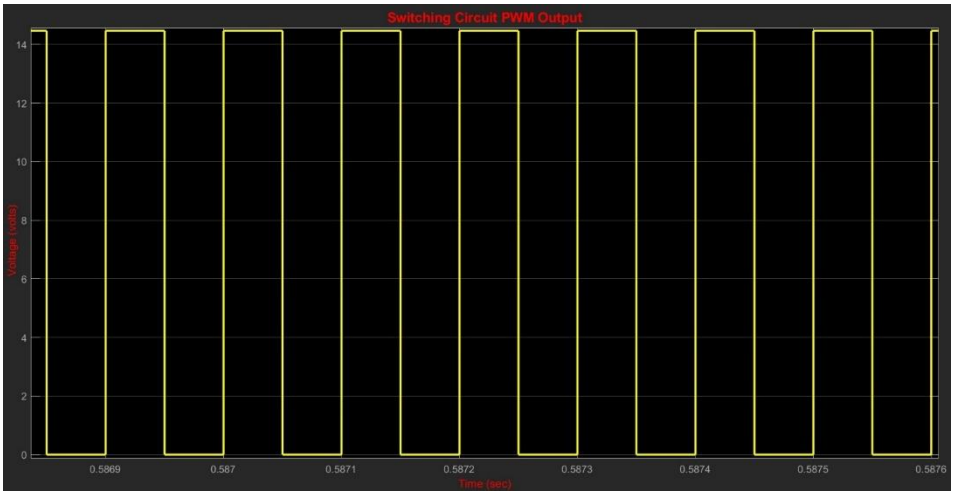

Figure 26: Switching Circuit PWM Output (Voltage (volts) vs Time (sec))

5. System Performance and Results

For testing the performance of the system, tuning the PD controller gains K_P , K_D process must be implemented. The tuning methodology described in Figure *20* was used and the setpoint was set to be 0.8mm. The first test was to measure the speed of the loop. To measure the speed of the loop, one of the microcontroller's digital pins was programmed to toggle its state at the end of every loop thus it will create square waves with the loop speed being half the period of the square wave as in Figure *27* The measured loop period is 306µs which is sufficient for updating the sensor and the controller output.

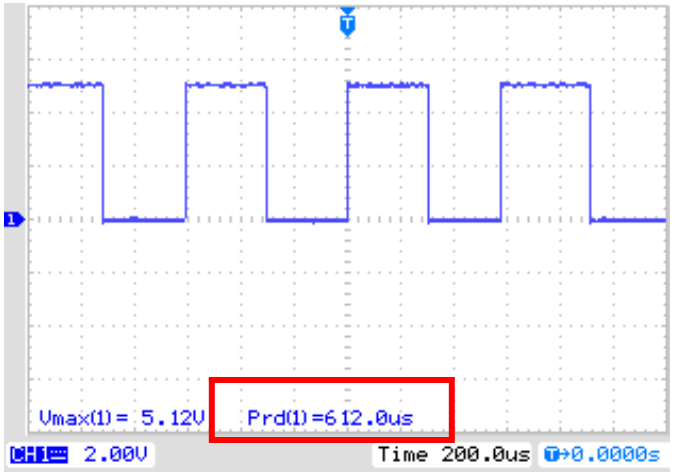

Figure 27 Toggled digital pin square wave (voltage (v) vs Time (sec)) which is used for measuring the loop period

The second test was to test the stability of the levitation at 0.8mm. The PD controller gains were configured with $K_P = 660$ *and* $K_D = 2650$. These values were obtained by applying the tuning methodology and many trails. However, the system did not reach a stable levitation. The air-gap length between ferromagnetic cores was unstable. Figure *28* shows the fluctuation in the length of the air-gap. The upper ferromagnetic core aggressively attracts the lower one leading to the 0mm reading and then let go which leads to the lower core to fall down to hit the safety clamps and the cycle repeats without stabilizing.

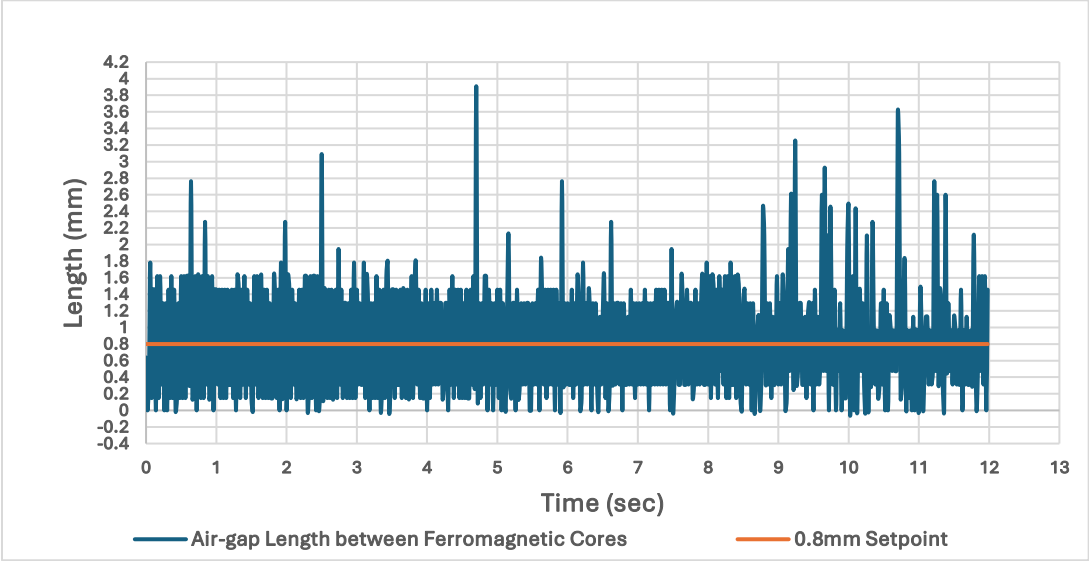

Figure 28 Air-gap length between the ferromagnetic cores of the implemented setup

Although many trails were carried, a stable response was never achieved. Troubleshooting the system thoroughly led to source of error in the system. The Hall-effect sensor measurements were very noisy which led to unstable controller response from the PD controller.

It is clear from **Error! Reference source not found.** that there is noise which disturbs the readings from the Hall-effect sensor. The spikes in the sensor measurements are interpreted by the controller that the table has fallen far away, thus huge error term will be produced. The controller will compensate for this big error by producing big output to reduce the gap between the ferromagnetic cores to the setpoint distance. The spikes can reach up to 4.79 V which is translated to 3.8mm false reading as in Figure *29*. The source of noise can be related to the interference from the power lines and any source of magnetic field present around the setup. To solve this problem another sensor must be considered as the limitations of Hall-effect sensors affected the performance of the setup severely.

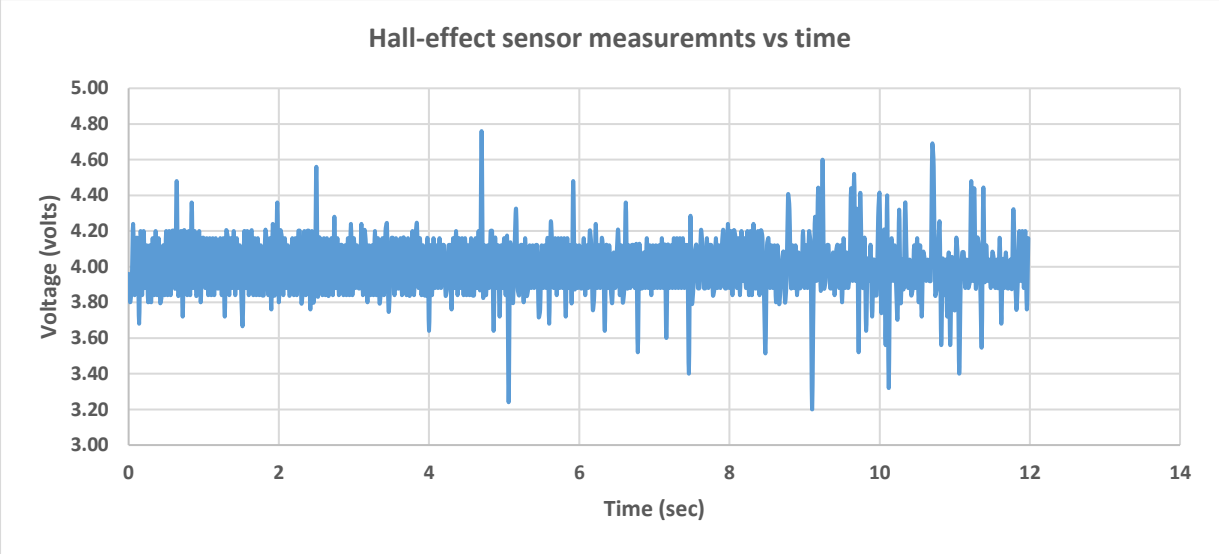

Figure 29 Hall-effect noisy measurements

6. Conclusion

Magnetic levitation systems are expensive and involve complex designs, which this work aimed to simplify. However, compared to other testing beds, they offer a more practical solution for simulating a frictionless environment, particularly for CubeSat ADCS testing. While they only replicate a frictionless condition along one axis, their potential can be greatly expanded when combined with components like a sun source, star catalog source, or vacuum chamber, enabling accurate and reliable testing for various scenarios.

Simulations demonstrated stable levitation at a 0.55 mm air gap; however, real-life implementation revealed limitations due to sensor noise, emphasizing the need for more accurate feedback solutions such as multiple Hall-effect sensors or optical displacement sensors. Further improvements, including larger electromagnet cores, electromagnetic dampers, and advanced control algorithms like sliding mode control, are recommended to enhance stability and performance.

This work highlights the potential of magnetic levitation systems for CubeSat ADCS testing and offers practical insights for advancing testbed design.

References

[1] F. Mier-Hicks and P. C. Lozano, "Electrospray thrusters as precise attitude control actuators for small satellites," *J. Guid. Control. Dyn.*, vol. 40, no. 3, pp. 642–649, 2017, doi: 10.2514/1.G000736.

[2] P. Balko and D. Rosinová, "Modeling of magnetic levitation system," no. June 2017, 2018, doi: 10.1109/PC.2017.7976222.

[3] A. Abbas and S. Z. Hassan, "Design and Control of Magnetic Levitation System," *2019 Int. Conf. Electr. Commun. Comput. Eng.*, no. July, pp. 1–5, 2019.

[4] F. M. Hicks, "Characterization on a magnetically levitated testbed for electrospray propulsion systems," *MIT Masters Thesis*, pp. 1–82, 2014.

[5] C. E. Lin and H. L. Jou, "Force Model Identification for Magnetic Suspension Systems via Magnetic Field Measurement," *IEEE Trans. Instrum. Meas.*, vol. 42, no. 3, pp. 767–771, 1993, doi: 10.1109/19.231612.

[6] J. Gilbert and R. Dewey, "Linear Hall-Effect Sensor ICS," *Allegro MicroSystems LLC*, 2013.

[7] Atmel *et al.*, "Harte und weiche Echtzeitsysteme Material zur Vorlesung Echtzeitsysteme I + II im Studienfach Technische Informatik an der," *Linux- Mag.*, no. November, p. 66, 2015, [Online]. Available: http://beagleboard.org/about%5Cnhttp://beagleboard.org/boards%5Cnhttps://www.raspberrypi.org/about/%5Cnhttp://redpitaya.com/about/%5Cnhttp://de.rs-online.com/web/p/digitalspeicher-oszilloskope/9010302/%5Cnhttp://www.linux-magazin.de/NEWS/Arduino-LLC-und-A.